ARTICLE

# Core−Shell Chromium Silicide−Silicon Nanopillars: A Contact Material for Future Nanosystems

**Mu-Tung Chang, Chih-Yen Chen, Li-Jen Chou,* and Lih-Juann Chen**

Department of Materials Science and Engineering, National Tsing Hua University, Hsinchu 300, Republic of China

**ABSTRACT** Chromium silicide nanostructures are fabricated inside silicon nanopillars grown by the vapor−liquid−solid mechanism. The remarkable field-emission behavior of these nanostructures results from extensive improvement of carrier transport due to the reduced energy barrier between the metal and semiconductor layers. The results warrant consideration of chromium silicide as a potentially important contact material in future nanosystems.

**KEYWORDS:** core−shell · chromium silicide · vapor−liquid−solid mechanism · field emission · nanopillars

In recent years, as the technology of microelectronics continues to scale down, one-dimensional (1D) nanostructures such as nanowires and nanotubes, representing an innovative vertically designed nanosystem, have attracted much attention for their fascinating properties and potential applications. This list includes nanologic devices,[1] light emitting diodes,[2] nanosensors,[4] and other devices for photovoltaics,[5] optoelectronic and spin-electronics,[6−8] and biomedical applications.[3] Semiconductor nanowires, including Si/Ge,[9,10] GaAs,[11] InAs,[12] and GaN,[13] are likely to supply the major building blocks of future nanoelectronic and nano-optoelectronic devices. The performance of 1-D nanofield effect transistor (FET) devices with complementary n- and p-type regions is comparable to the best performance of planar devices fabricated from the same materials.[14] As in the standard FET mechanism, a semiconductor nanowire as the building block of an integrated logic device is connected to the source and drain electrodes. The interface between semiconductor and electrode is critical to device performance. Metal silicides are ideal candidates for the interconnects, or nanocontacts, owing to their low resistivity, ohmic contact to both p- and n-type semiconductors, stability at high temperatures, low cost, and compatibility with Si complementary metal-oxide-semiconductor (CMOS) device processing.[15] Wu *et al.* have demonstrated the fabrication of metallic nickel silicide/silicon nanowire heterostructures as nanocontacts in a nano-FET device.[16] To date, nickel silicide nanowires have been shown to act as excellent interconnections.[17,18] Titanium and tantalum silicide nanowires[19,20] have also been successfully synthesized.

The growth mechanisms of semiconductor nanowires include the vapor−solid (VS), vapor−liquid−solid (VLS), and oxide-assisted growth (OAG)[21−23] approaches. Of these, VLS has been regarded as the most promising because the size and location of the nanowires can be precisely controlled by the metal catalysts. VLS depends on the metal catalyst reaching supersaturation at elevated temperatures. When the temperature fluctuates, nanowire can be grown from the catalyst at the tip area. However, the Schottky barrier is often a problem at the interface between metal and semiconductor, degrading the electrical performance of the nanodevice.[24] Herein, we demonstrate a novel nanostructure that addresses this issue: chromium silicide nanopillar embedded in a Si nanorod.

In this study we use the VLS method to fabricate core−shell chromium silicide nanopillars inside silicon nanorods using a gold tip. We use field emission to compare the transport behavior of silicon nanorods with and without the embedded nanopillar; our field emission study shows the calculated field enhancement factor β of the metal silicide nanopillars in the Si nanorods over pure Si nanorods is approximately 2500, presumably due to a reduced potential barrier for electron tunneling. The maxi-

*Address correspondence to ljchou@mx.nthu.edu.tw.

Received for review August 20, 2009 and accepted October 26, 2009.

**Published online October 29, 2009.** 10.1021/nn901045f CCC: $40.75

mum current density of the silicide/Si nanostructure is more than 2 orders of magnitude higher than that of pure Si nanorod. The significant improvement in field-emission behavior demonstrates that metal silicide nanopillars embedded in the Si nanorods could act as an outstanding nanocontact material in future vertical nanodevices. Moreover, this mechanism can be extended to the other metal silicide systems, such as β-iron disilicide or erbium silicide, for application to photogeneration nanodevices.

## RESULTS AND DISCUSSION

Figure 1a shows an SEM image of pure Si nanorods synthesized by the evaporation of silicon on gold-coated silicon substrate at 600 °C for 3 h. High-density and uniform distribution of vertically aligned Si nanorods were achieved. The length of the nanorods can be extended to 400−600 nm, with diameters ranging from 80 to 120 nm. They are hexagonal in cross-section, with metal catalysts at the tip areas, and were grown directly on Si substrate (inset, Figure 1a). Pinholes with {111} facets were observed to surround the Si nanorods, indicating that Si atoms diffused to the tip area during growth of the nanorods. Figure 1b shows a TEM image of the Si nanorod. Figure 1c is an enlarged view of the highlighted region in Figure 1b, showing the single crystal structure with no evidence of defects. The corresponding selected area diffraction pattern (SAD) (inset of Figure 1b) and high-resolution TEM image confirm that the spacing of 0.32 nm can be ascribed to the Si(111) plane with the growth direction along the Si[111].

Figure 2a shows an SEM image of the nanorods formed by codeposition of the Si and Cr sources on gold-coated silicon substrate. The surface was rough because of the low migration velocity of chromium atoms on silicon. A TEM image of a Si/silicide nanostructure is shown in Figure 2b. In Figure 2c, a high-resolution TEM image shows the epitaxial interface between silicon and silicide. The two *d* spacings of 0.32 and 0.65 nm correspond to the Si{111} and $Cr_5Si_3${110} planes, respectively.[25] Insets in the corner display the corresponding SAD patterns of Si nanorod and metal silicide nanostructure, respectively. Based on these high-resolution TEM images and SAD patterns, the growth direction of the Si/silicide nanostructure is along the direction of Si[111]; the epitaxial relationship between the silicon and silicide is Si(111) parallel to $Cr_5Si_3$(110). In Figure 2d, the corresponding elemental line-scan mapping of the nanorod obtained in the STEM mode indicates that the chromium silicide is embedded in the silicon and is also confirmed by the EDS spectrum data (Figure 2e).

Surface energy plays an important role in nanoscale phenomena such as formation of various nanostructures, growth direction of 1D nanomaterials and shape transformation of nanoparticles. Surface energy

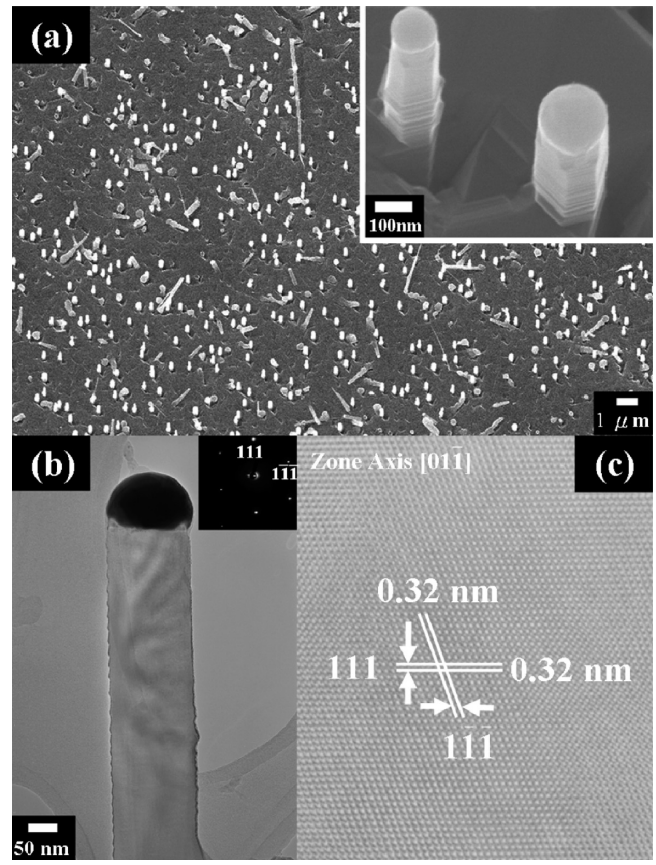


**Figure 1. (a) SEM image of large-scale Si nanorods; inset in the upper-left corner shows enlarged image of two nanorods. (b) TEM image of a Si nanorod; inset shows corresponding selected area diffraction pattern. (c) Magnified view of the outlined region of panel b.**

may also play a pivotal role in the growth of core−shell nanostructures. In a previous study, the modified analytic embedded atom method (MAEAM) was developed to estimate the relative surface energies of metal elements, several of which are listed in Table 1.[26] To minimize overall surface energy, elements with lower surface energies tend to cover those with higher surface energies. In our case, as the chromium atoms are continually impinging onto the gold catalyst, they tend to agglomerate around the central region of the growing nanowire. The chromium silicide is produced by reaction of the chromium atoms with the silicon matrix and embedded in the Si nanorod. Silicide-silicon core−shell nanostructures may be formed by a similar mechanism in the case of any metal with a surface energy higher than that of the gold, such as Fe or Ni.

A growth model of the core−shell nanostructures and their corresponding energy levels is schematically illustrated in Figure 3, where the Si Fermi level ($E_F$) is equal to the intrinsic Fermi level ($E_i$). The energy band diagram for the gold catalyst and silicon before contact is shown in Figure 3a, for which the gold work function and Si electron affinity are 5.1 and 4.01 eV, respectively. The thermal-equilibrium metal−semiconductor (M−S) band diagram for this case is illustrated in Figure 3b. After the chromium silicide nanopillars are

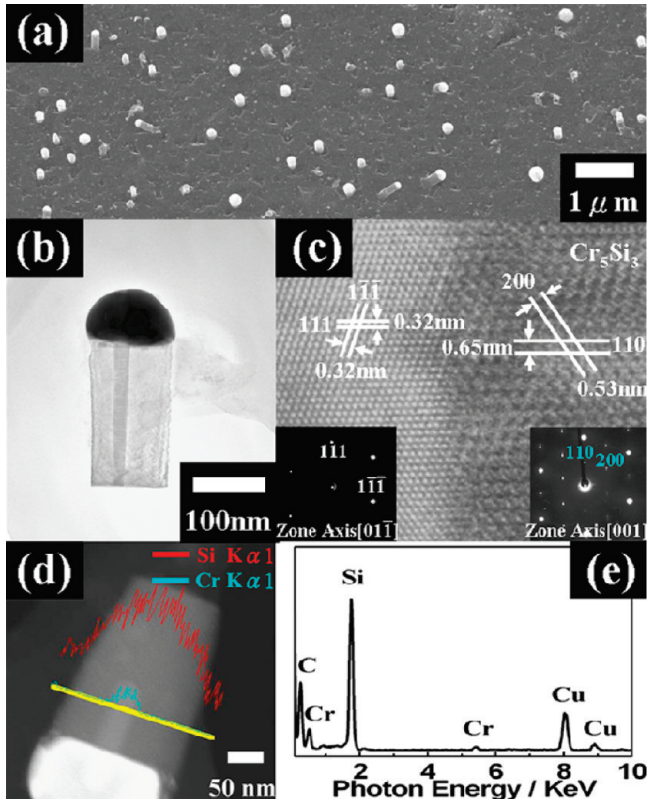


**Figure 2. (a) SEM image of a nanopillar embedded in a Si nanorod. (b) TEM image of the core−shell nanostructure. (c) High-resolution TEM image of the nanostructure; insets at the bottom left and right corners are the corresponding selected area diffraction patterns of Si nanorod and metal silicide nanostructure, respectively. (d) The elemental line-scan mapping of the nanorod obtained in the STEM mode. (e) The corresponding EDS spectrum.**

formed, the M−S junction becomes silicon−silicide instead of Au−Si, as shown in Figure 3c. Chromium silicide is a satisfactory material for a nanocontact, with a work function of 3.8 eV, which is smaller than that of Si (4.01 eV). As a result, the image-force-induced lowering of the Schottky barrier[27] forms an outstanding ohmic contact, easing the carrier (electron) transport through the M−S junction significantly.

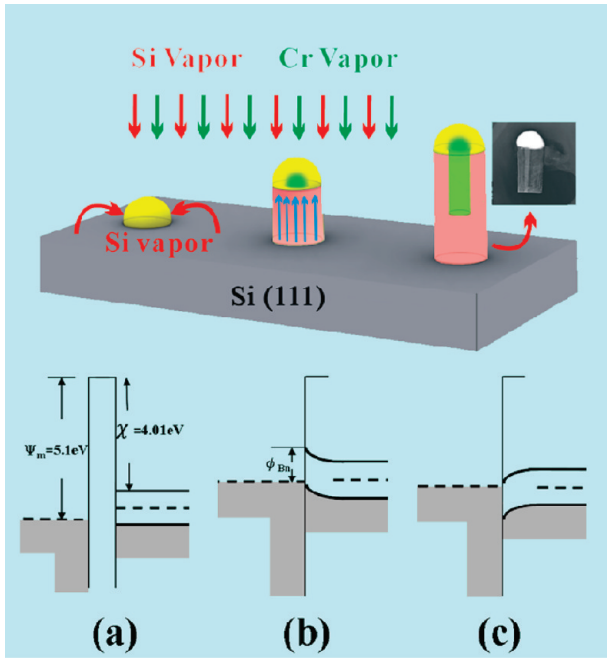


**Figure 3. Growth model schematics and corresponding energy band diagrams.**

**TABLE 1. Surface Energies of Various Metals Calculated Using the MAEAM in Reference 26**

| surface energy (ergs/cm$^2$) | (100) | (110) | (111) | (210) | (211) |
|---|---|---|---|---|---|
| Au | 713.2 | 794.0 | 639.8 | 841.2 | 761.7 |
| Cr | 1461 | 3979 | 3505 | 1496 | 1554 |
| Ni | 1305 | 1417 | 1170 | 1493 | 1371 |
| Fe | 1537 | 2222 | 2430 | 1595 | 1662 |

Figure 4 shows the relationship between current density and applied electric field at a distance of 150 μm between anode and sample. Figure 4 panels a and b illustrate the results for silicide/Si nanostructure and pure Si nanorod, respectively, while the aspect ratios of these are almost the same *via* the process control. The maximum current density of the silicide/Si nanostructure is higher than that of pure Si nanorod. This divergence may be attributed to the introduction of metallic silicide, which effectively provides a shortcut as the electrons pass though the interface between the gold-catalyst and Si. The insets of Figure 4 show the corresponding Fowler−Nordheim plot (ln ($J/E^2$)−1/$E$ curve), and the F−N relationship can be given as[28]

$$J = \left(\frac{A\beta^2E^2}{\Phi}\right)\exp\left(\frac{-B\Phi^{3/2}}{\beta E}\right)$$

where $J$ is the current density, $E$ is the applied field strength, and $\Phi$ is the work function. $A$ and $B$ are constant, corresponding to $1.56 \times 10^{-10}$ [AV$^{-2}$ (eV)] and $6.83 \times 10^3$ [V (eV$^{-3/2}$) (μm$^{-1}$)], respectively. The field enhancement factor, reflecting the degree of field emission for the tip shape on a planar surface, can be estimated from the slope ($-B\Phi^{3/2}/\beta$) of the F−N plot. At high field, the straight lines reflecting the β values can be clearly seen, indicating that the barrier-tunneling mechanism is responsible for the field emission phenomenon. According to these measurements, the calculated β value of the metal silicide nanopillars in the Si nanorods is around 2500, considerably higher than the pure Si nanorod, due to the reduced potential barrier for the electron tunneling. The maximum current density of the silicide/Si nanostructure is more than 2 orders of magnitude higher than that of pure Si nanorod. The phenomenally enhanced field emission behavior of these core−shell silicide/silicon nanostructures provides a new solution for future nanocontacts in vertically designed nanoelectronics and optoelectronics.

## CONCLUSION

In summary, novel core−shell chromium silicide nanostructures are fabricated inside silicon nanopil-

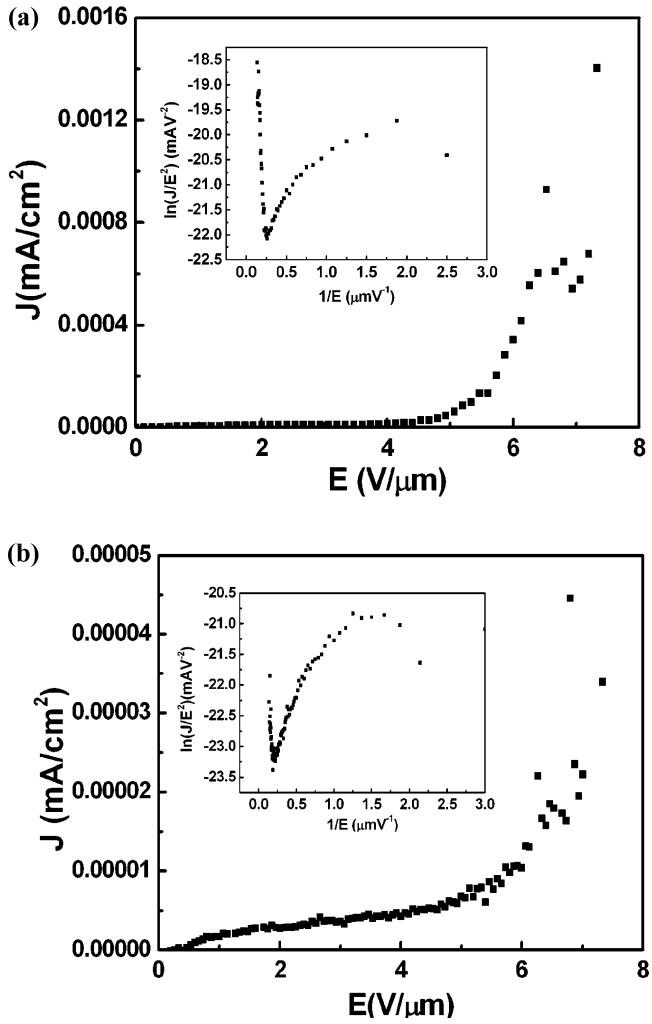


**Figure 4. Electron field-emission behavior of (a) silicide/Si nanostructures and (b) pure Si nanorods.**

lars grown by the vapor−liquid−solid mechanism, where surface energy plays an important role in the formation of nanostructures. The remarkable field-emission behavior of these nanostructures demonstrates extensive improvement of carrier transport due to the reduced energy barrier between the metal and semiconductor shells. The results indicate a potentially important application for chromium silicide as a contact material in future nanosystems.

## EXPERIMENTAL SECTION

Single crystal (111) Si wafer (1−30 Ω-cm) was cleaned by the standard process and a 2-nm-thick Au film was deposited on the Si substrate in a high-vacuum e-beam deposition system at room temperature. The as-deposited sample was then dipped into dilute HF and immediately loaded into an ultrahigh-vacuum chamber. The sample was then transferred into a molecular beam epitaxy (MBE) chamber equipped with an electron gun for Si evaporation and an effusion cell for chromium deposition. For TEM analysis, the products were dispersed by sonication in isopropyl solution, and subsequently transferred onto a copper grid covered with porous carbon films. A field-emission transmission electron microscope (JEM-3000F, operated at 300 kV with a point-to-point resolution of 0.17 nm) equipped with an energy dispersive spectrometer (EDS) was used to obtain the data on microstructure and chemical composition. The Z-contrast images were obtained by a high-angle annular dark-field (HAADF) detector to detect electrons scattered at high angles. The surface morphology was examined with a field-emission scanning electron microscope (JSM-6500F) operating at 15 kV. Finally, electron field-emission properties were measured in a vacuum better than $1 \times 10^{-6}$ Torr using an indium tin oxide (ITO) plate as the anode. The lowest emission current was recorded on the order of nA. The measurement distance between the anode and emitting surface was fixed at 150 μm.

*Acknowledgment.* This research was supported by the National Science Council through Grant Nos. NSC 95-2221-E-007-245-MY2 and NSC 96-ET-7-007-002-ET.

## REFERENCES AND NOTES

1. Yang, C.; Zhong, Z.; Lieber, C. M. Encoding Electronic Properties by Synthesis of Axial Modulation-Doped Silicon Nanowires. *Science* **2005**, *310*, 1304–1307.

2. Qian, F.; Li, Y.; Gradečak, S.; Wang, D.; Barrelet, C.; Lieber, C. M. Gallium Nitride-Based Nanowire Radial Heterostructures for Nanophotonics. *Nano Lett.* **2004**, *4*, 1975–1979.
3. Cui, Y.; Wei, Q.; Park, H.; Lieber, C. M. Nanowire Nanosensors for Highly Sensitive and Selective Detection of Biological and Chemical Species. *Science* **2001**, *293*, 1289–1292.
4. Wang, X. D.; Summers, C. J.; Wang, Z. L. Large-Scale Hexagonal-Patterned Growth of Aligned ZnO Nanorods for Nano-optoelectronics and Nanosensor Arrays. *Nano Lett.* **2004**, *4*, 423–426.
5. Kelzenberg, M. D.; Turner-Evans, D. B.; Kayes, B. M.; Filler, M. A.; Putnam, M. C.; Lewis, N. S.; Atwater, H. A. Photovoltaic Measurements in Single-Nanowire Silicon Solar Cells. *Nano Lett.* **2008**, *8*, 710–714.
6. Chang, M. T.; Chou, L. J.; Chueh, Y. L.; Lee, Y. C.; Hsieh, C. H.; Chen, C. D.; Lan, Y. W.; Chen, L. J. Nitrogen-Doped Tungsten Oxide Nanowires: Low Temperature Synthesis on Si and the Electrical, Optical, and Field-Emission Properties. *Small* **2007**, *3*, 658–664.
7. Chang, M. T.; Chou, L. J.; Hsieh, C. H.; Chueh, Y. L.; Wang, Z. L.; Murakami, Y.; Shindo, D. Magnetic and Electrical Characterizations of the Half-Metallic Magnetite ($Fe_3O_4$) Nanowires. *Adv. Mater.* **2007**, *19*, 2290–2294.
8. Hsieh, C. H.; Chou, L. J.; Lin, G. R.; Bando, Y.; Golberg, D. Nano-photonic Switch: Gold-in-$Ga_2O_3$ Peapod Nanowires. *Nano Lett.* **2008**, *10*, 3081–3085.
9. Chueh, Y. L.; Chou, L. J.; Cheng, S. L.; He, J. H.; Chen, L. J. Synthesis of Taperlike Si Nanowires with Strong Field Emission. *Appl. Phys. Lett.* **2005**, *86*, 133112–133115.
10. Xiang, J.; Lu, W.; Hu, Y. J.; Wu, Y.; Yan, H.; Lieber, C. M. Ge/Si Nanowire Heterostructures as High Performance Field-Effect Transistors. *Nature* **2006**, *441*, 489–493.
11. Duan, X. F.; Wang, J. F.; Lieber, C. M. Synthesis and Optical Properties of Gallium Arsenide Nanowires. *Appl. Phys. Lett.* **2000**, *76*, 1116–1118.
12. Jensen, L. E.; Bjork, M. T.; Jeppesen, S.; Persson, A. I.; Ohlsson, B. J.; Samuelson, L. Role of Surface Diffusion in Chemical Beam Epitaxy of InAs Nanowires. *Nano Lett.* **2004**, *4*, 1961–1964.
13. Hsieh, C. H.; Chang, M. T.; Chien, Y. J.; Chou, L. J.; Chen, L. J.; Chen, C. D. Coaxial Metal−Oxide-Semiconductor (MOS) Au/$Ga_2O_3$/GaN Nanowires. *Nano Lett.* **2008**, *10*, 3288–3292.
14. Zheng, G. F.; Lu, W.; Jin, S.; Lieber, C. M. Synthesis and Fabrication of High-Performance N-Type Silicon Nanowire Transistors. *Adv. Mater.* **2004**, *16*, 1890–1893.
15. Chen, L. J. Metal Silicides: An Integral Part of Microelectronics. *J. Met., Mater. Miner.* **2005**, *57* (9), 24–30.
16. Wu, Y.; Xiang, J.; Yang, C.; Lu, W.; Lieber, C. M. Single-Crystal Metallic Nanowires and Metal/Semiconductor Nanowire Heterostructures. *Nature* **2004**, *430*, 61–65.
17. Dong, L. F.; Bush, J.; Chirayos, V.; Solanki, R.; Jiao, J.; Ono, Y.; Conley, J. F., Jr.; Ulrich, B. D. Dielectrophoretically Controlled Fabrication of Single-Crystal Nickel Silicide Nanowire Interconnects. *Nano Lett.* **2005**, *5*, 2112–2115.
18. Song, Y. P.; Schmitt, A. L.; Jin, S. Ultralong Single-Crystal Metallic $Ni_2Si$ Nanowires with Low Resistivity. *Nano Lett.* **2007**, *7*, 965–969.
19. Hsu, H. C.; Wu, W. W.; Hsu, H. F.; Chen, L. J. Growth of High-Density Titanium Silicide Nanowires in a Single Direction on a Silicon Surface. *Nano Lett.* **2007**, *7*, 885–889.
20. Kim, J. J.; Shindo, D.; Murakami, Y.; Chou, L. J.; Chueh, Y. L. Direct Observation of Field Emission in a Single $TaSi_2$ Nanowire. *Nano Lett.* **2007**, *7*, 2243–2247.
21. Chueh, Y. L.; Ko, M. T.; Chou, L. J.; Chen, L. J.; Wu, C. S.; Chen, C. D. $TaSi_2$ Nanowires: A Potential Field Emitter and Interconnect. *Nano Lett.* **2006**, *6*, 1637–1644.
22. Chueh, Y. L.; Chou, L. J.; Hsu, C. A.; Kung, S. C. Synthesis and Characterization of Taper- and Rodlike Si Nanowires on $Si_xGe_{1-x}$ Substrate. *J. Phys. Chem. B* **2005**, *109*, 21831–21835.
23. Lee, S. T.; Wang, N.; Zhang, Y. F.; Tang, Y. H. Oxide-Assisted Semiconductor Nanowire Growth. *MRS Bull.* **1999**, *24*, 36–42.
24. Weber, W. M.; Geelhaar, L.; Graham, A. P.; Unger, E.; Duesberg, G. S.; Liebau, M.; Pamler, W.; Cheze, C.; Riechert, H.; Lugli, P.; Kreupl, F. Silicon-Nanowire Transistors with Intruded Nickel-Silicide Contacts. *Nano Lett.* **2006**, *6*, 2660–2666.
25. Dauben, C. H.; Templeton, D. H.; Myers, C. E. The Crystal Structure of $Cr_5Si_3$. *J. Phys. Chem.* **1956**, *60*, 443–445.
26. Wen, Y. N.; Zhang, H. M. Surface Energy Calculation of the FCC Metals by Using the MAEAM. *Solid State Commun.* **2007**, *144*, 163–167.
27. Neamen, Donald A. *Semiconductor Physics and Devices,* 3rd ed.; Irwin: Chicago, IL, 2005; Chapter 8, p 307.
28. Fowler, R. H.; Nordheim, L. W. Electron Emission in Intense Electric Fields. *Proc. R. Soc. London, A* **1928**, *119*, 173–181.